

A Simple Model for Lensing by Black Holes in Galactic Nuclei

M.C. Werner^{*} and N.W. Evans^{*}

Institute of Astronomy, University of Cambridge, Madingley Road, Cambridge, CB3 0HA, United Kingdom

This draft 2006 February 13

ABSTRACT

The lensing properties of the Plummer model with a central point mass and external shear are derived, including the image multiplicities, critical curves and caustics. This provides a simple model for a flattened galaxy with a central supermassive black hole. For the Plummer model with black hole, the maximum number of images is 4, provided the black hole mass is less than an upper bound which is calculated analytically. This introduces a method to constrain black hole masses by counting images, thus applicable at cosmological distance. With shear, the maximum number of images is 6 and we illustrate the occurrence of an astroid caustic and two metamorphoses.

Key words: gravitational lensing, black holes

1 INTRODUCTION

Albert Einstein, in his 1911 paper *On the Influence of Gravitation on the Propagation of Light*, applied the principle of equivalence to the deflection of light rays by the sun. This marks the beginning of our modern understanding of gravitational lensing. After the full prediction from General Relativity had been confirmed by Eddington's observations of the 1919 solar eclipse, it was only in 1936 that Einstein considered, rather pessimistically, the deflection due to stars. Zwicky's (1937) insight one year later that galaxies were much better candidates was finally corroborated by the discovery of the first doubly-lensed quasar in 1979 by Walsh, Carswell and Weymann.

Nowadays, over a 100 multiply imaged gravitational lens systems are known. In many of these, a background quasar or radio galaxy is lensed into doublets or quadruplets by an early-type galaxy. Provided the density distribution at the centre of the lensing galaxy is weakly singular (that is, no worse than $\rho \sim 1/r$), then gravitational lensing yields an odd number of images, generally three or five. If the singularity is stronger than this, then there is an even number of images, as the central image is absent (Evans & Wilkinson 1998). Most early-type galaxies are believed to harbour supermassive black holes in their centres. The existence and the magnification of the central image in gravitational lens systems are very sensitive to the mass distribution in the centre and the presence of a black hole. Keeton (2003) has shown that the likely range of the flux of any central image is below the range of current instruments, but within the grasp of forthcoming, high sensitivity VLBI arrays. Thus, it is becoming possible to probe the mass distribution in the central tens of parsecs of the lensing galaxy. It is therefore worthwhile to develop some simple models of lensing by galaxies with black holes. Mao et al. (2001) already studied a galaxy model akin to the cored isothermal sphere and showed that a central black

hole – provided it is not too massive – can create an additional faint central image.

The present paper is a mainly analytical study of the Plummer lens with a central black hole and in the presence of external shear. In §2, we briefly review the properties of the spherical Plummer lens and show that its images obey a magnification invariant. This model is extended in §3 to include a central point mass to which external shear is added in §4.

2 THE PLUMMER MODEL

Plummer's (1911) model is the simplest self-consistent solution of the collisionless Boltzmann equation with finite total mass. Although the density in early-type galaxies decreases less steeply than $\rho \sim r^{-5}$ at large radii, the Plummer model still gives a good description of the inner parts, which control the lensing properties.

For an isotropic stellar system, the distribution function f depends on the (negative) total particle energy E only. The Plummer model is then a polytrope defined by the distribution function

$$f(E) \propto (-E)^{7/2}. \quad (1)$$

For a static system, energy conservation $E = \phi + \mathbf{v}^2/2$ holds and, as a consequence, Poisson's equation for a self-consistent, self-gravitating, spherical and isotropic system

$$\frac{1}{r^2} \frac{d}{dr} \left(r^2 \frac{d\phi}{dr} \right) = 16\pi^2 G \int f(E) v^2 dv \quad (2)$$

implies the mass density (e.g. Binney & Tremaine 1994, p. 225)

$$\rho = \rho_0 \left(1 + \left(\frac{r}{r_0} \right)^2 \right)^{-5/2} \quad (3)$$

and total mass $M = 4\pi\rho_0 r_0^3/3$.

^{*} E-mail: mcw36@ast.cam.ac.uk; nwe@ast.cam.ac.uk

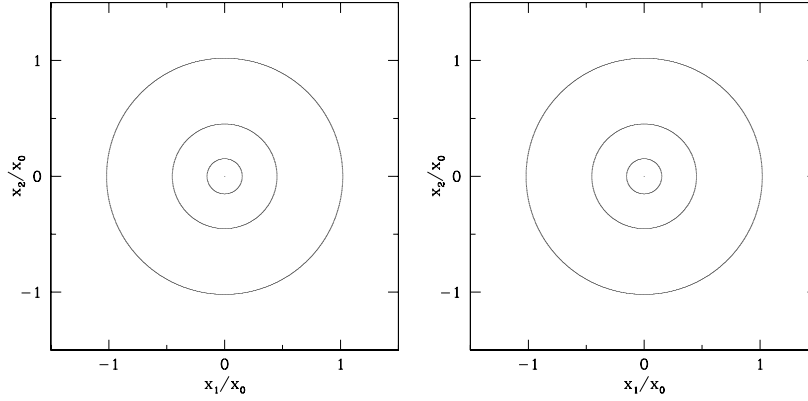


Figure 1. Plummer lens with central point mass, $\kappa_0 = 2$, $a_0 = 0.02$. Left: critical circles in L , right: caustic circles in S . Number labels indicate number of images.

2.1 Lens Equation

The angular diameter distances from the observer to the lens plane L , the source plane S and from L to S be denoted by D_{LO}, D_{SO} and D_{SL} , respectively. We use the conventional dimensionless coordinates \mathbf{x} in L and \mathbf{y} in S (see e.g., Schneider et al. 1999, p. 245). The relative surface density κ_P is now obtained by projecting (3) onto L ,

$$\kappa_P = \kappa_0 \left(1 + \left(\frac{x}{x_0} \right)^2 \right)^{-2} \quad (4)$$

where $x = |\mathbf{x}|$ such that the origin coincides with the lens centre, $x_0 = r_0/D_{LO}$ and

$$\kappa_0 = \frac{M}{\pi r_0^2 \Sigma_{\text{crit}}}, \quad \Sigma_{\text{crit}} = \frac{c^2 D_{SO}}{4\pi G D_{SL} D_{LO}}. \quad (5)$$

The deflection potential Ψ is

$$\Psi_P = \Psi_0 + \frac{\kappa_0 x_0^2}{2} \ln \left(1 + \left(\frac{x}{x_0} \right)^2 \right). \quad (6)$$

The lens equation is then

$$\mathbf{y} = \mathbf{x} - \nabla \Psi_P = \mathbf{x} - \frac{\kappa_0 \mathbf{x}}{1 + \left(\frac{x}{x_0} \right)^2}. \quad (7)$$

The image and caustic properties of the Plummer lens are briefly summarized below, for comparison with our results in §3 and §4

2.2 Image and Caustic Properties

The determinant of the Jacobian of the Plummer lens map is

$$\det J = \left(1 - \frac{\kappa_0}{1 + \left(\frac{x}{x_0} \right)^2} \right)^2 + \left(1 - \frac{\kappa_0}{1 + \left(\frac{x}{x_0} \right)^2} \right) \frac{2\kappa_0 \left(\frac{x}{x_0} \right)^2}{\left(1 + \left(\frac{x}{x_0} \right)^2 \right)^2}. \quad (8)$$

The origins of L and S are critical and caustic points, respectively. For a point source at the origin $\mathbf{y} = 0$, the lens equation implies a circular image, the Einstein ring, with radius $x = x_0 \sqrt{\kappa_0 - 1}$ and infinite magnification. Otherwise, without loss of generality, let the source position be $\mathbf{y} = (y_1, 0)$, whence $x_2 = 0$ and

$$x_1^3 - y_1 x_1^2 + (1 - \kappa_0) x_0^2 x_1 - x_0^2 y_1 = 0. \quad (9)$$

Thus, there are one or three images, depending on the source position y_1 . The images lie on a straight line through the lens centre.

For $y_1 \rightarrow \infty$, $J \rightarrow \mathbf{I}$ (the identity matrix), so there is always one image at large y_1 , as expected.

The critical curves can be obtained from (8) with $\det J = 0$ resulting in

$$\begin{aligned} x_{\text{crit},1} &= x_0 \sqrt{\kappa_0 - 1} \\ x_{\text{crit},2} &= x_0 \sqrt{\frac{\kappa_0}{2} \sqrt{1 + \frac{8}{\kappa_0}} - \left(1 + \frac{\kappa_0}{2} \right)}. \end{aligned}$$

There are two critical circles in L if $\kappa_0 > 1$. Applying the lens equation then shows that the caustic corresponding to $x_{\text{crit},1}$ is the origin point in S , whereas the other caustic is circular, as expected by symmetry. Hence three images can occur by crossing this caustic inwards. However, if $\kappa_0 \leq 1$ then only a critical and caustic point exist and the number of images is one for all $\mathbf{y} \neq 0$.

2.3 Magnification Invariant

Witt & Mao's (1995) paper introduced the notion of a lensing invariant. They considered a binary lens of two point masses. Their main result is that the sum of the signed magnifications of the maximum number of five images is unity, namely

$$\sum_{i=1}^5 \mu_i p_i = 1. \quad (10)$$

Here, μ_i is the absolute magnification of the image, while p_i is the parity. This result holds good irrespective of the position of the source, provided it remains within the central caustic giving rise to the maximum number of images. Subsequently, Rhie (1997) and Witt & Mao (2000) found further examples of lens models with invariants. A general theory of such invariants using single variable complex analysis (Hunter & Evans 2001; Evans & Hunter 2002; An & Evans 2006) was developed. This approach is used here to investigate the general circularly symmetric lens and, in particular, the Plummer model.

2.3.1 Circular Symmetric Lenses

The standard complexification is introduced (e.g. Petters, Levine & Wambsganss 2001, chap. 15.1). Let L_c , S_c be the complex lens and source planes, respectively, and define the complex coordinates

$$z = x_1 + ix_2 \in L_c, \quad \zeta = y_1 + iy_2 \in S_c. \quad (11)$$

Let the complex conjugate be denoted by a bar. The complex lens equation is rendered

$$\zeta = z - zf(z\bar{z}), \quad (12)$$

where the deflection factor f is

$$f(s) = 2 \frac{d\Psi(s)}{ds}. \quad (13)$$

Note that, by definition, f is a real-valued function so that $\bar{f} = f$. The conjugate of the lens equation is therefore

$$\bar{\zeta} = \bar{z} - \bar{z}f(z\bar{z}) \quad (14)$$

and so

$$\bar{z} = \frac{z\bar{\zeta}}{\zeta}. \quad (15)$$

The geometrical meaning of (15) is plain: due to circular symmetry, we can without loss of generality orientate the real axes in S_c , L_c so that the source position $\zeta = \bar{\zeta}$ is real and hence, by (15), the image positions as well: lens centre, point source and all images are collinear. Also, (15) allows us to eliminate \bar{z} from the lens equation (12) so that standard, one-dimensional complex analysis may be applied. It can be recast thus to give the imaging equation

$$I(z_i, \zeta, \bar{\zeta}) = 0, \quad (16)$$

defined so that image positions z_i correspond to the roots of

$$I(z, \zeta, \bar{\zeta}) = z - zf\left(\frac{z^2\bar{\zeta}}{\zeta}\right) - \zeta. \quad (17)$$

As the lens model f may have isolated poles in the complex plane, the imaging equation is meromorphic.

The signed flux magnification of the image at z_i is given by (e.g., Petters et al. 2001, p. 85)

$$\mu_i = \frac{1}{\det J(z_i)}, \quad (18)$$

where the Jacobian J and its inverse J^{-1} in complex form can be written as (e.g., Petters et al. 2001, p. 506)

$$J = \begin{pmatrix} \frac{\partial \zeta}{\partial z}|_{\bar{z}} & \frac{\partial \zeta}{\partial \bar{z}}|_z \\ \frac{\partial \bar{\zeta}}{\partial z}|_{\bar{z}} & \frac{\partial \bar{\zeta}}{\partial \bar{z}}|_z \end{pmatrix}, \quad J^{-1} = \begin{pmatrix} \frac{\partial z}{\partial \zeta}|_{\bar{\zeta}} & \frac{\partial z}{\partial \bar{\zeta}}|_{\zeta} \\ \frac{\partial \bar{z}}{\partial \zeta}|_{\bar{\zeta}} & \frac{\partial \bar{z}}{\partial \bar{\zeta}}|_{\zeta} \end{pmatrix}.$$

Requiring that $JJ^{-1} = I$, it follows that

$$\det J = \frac{\frac{\partial \bar{\zeta}}{\partial z}|_z}{\frac{\partial \zeta}{\partial \bar{z}}|_{\bar{z}}}. \quad (19)$$

By standard calculus, we find that the sum of the signed magnifications of the N images is

$$\sum_{i=1}^N \mu_i = \sum_{i=1}^N \frac{1}{\det J(z_i)} = \sum_{i=1}^N \frac{-\frac{\partial I}{\partial \zeta}|_{\bar{\zeta}, z}}{\frac{\partial I}{\partial z}|_{\zeta, \bar{\zeta}} \frac{\partial \bar{\zeta}}{\partial \bar{z}}|_z}. \quad (20)$$

By using (12) in the denominator and (16) in the numerator of (20), the following simplification is obtained

$$\sum_{i=1}^{N_{max}} \mu_i = \sum_{i=1}^{N_{max}} \frac{z_i}{\zeta \frac{\partial I}{\partial z}|_{\zeta, \bar{\zeta}}}. \quad (21)$$

We now seek a complex-valued function with residues of the form (21). Consider the integral of

$$F(z, \zeta, \bar{\zeta}) = \frac{z}{(\zeta + I)I}, \quad (22)$$

along a contour \mathcal{C} enclosing all N_{max} roots z_i . Assuming that the roots of the imaging equations are simple, the integrand F has a simple pole at each root of I and hence residues

$$\text{res}(F; z_i) = \frac{z_i}{\zeta \frac{\partial I}{\partial z}|_{\zeta, \bar{\zeta}}(z_i)}, \quad (23)$$

by Taylor expansion of I about z_i , as required. Now from the residue theorem, we find

$$\sum_{i=1}^N \mu_i = \sum_{i=1}^N \text{res}(F; z_i) = \frac{1}{2\pi i} \oint_{\mathcal{C}} \frac{z}{(\zeta + I)I} dz. \quad (24)$$

Furthermore, two assumptions are made which both restrict the functions f . First, no branch cuts to ensure singlevaluedness of I are to occur, such that the complex plane is analytic everywhere outside \mathcal{C} . Secondly, it is assumed that the deflection angle becomes negligible at large distance from the lens centre. This amounts to $\nabla\Psi \rightarrow 0$ as $x \rightarrow \infty$, hence $zf \rightarrow 0$ and therefore $I \rightarrow z$ as $|z| \rightarrow \infty$. Then by Cauchy's theorem, \mathcal{C} can be distorted to a circle at infinity \mathcal{C}_{∞}

$$\sum_{i=1}^{N_{max}} \mu_i = \frac{1}{2\pi i} \oint_{\mathcal{C}_{\infty}} \frac{z}{(\zeta + I)I} dz = \frac{1}{2\pi i} \oint_{\mathcal{C}_{\infty}} \frac{dz}{z} = 1. \quad (25)$$

This result is a magnification invariant for the maximum number of roots N_{max} of the imaging equation.

Although each image corresponds to a complex root of the imaging equation, there may exist roots which do not correspond to physical images and which are therefore called spurious roots. To understand their impact on (25), consider two of their properties. First, by choosing without loss of generality $\zeta = \bar{\zeta}$ in the imaging equation (16), it is seen that both z and \bar{z} are solutions. So, all spurious roots occur as complex conjugate pairs. Secondly, from (16) and (21), we see that the magnifications of a pair of conjugate spurious roots are also complex conjugate. This implies that the total contribution from spurious roots to the signed magnification sum is always real.

2.3.2 The Particular Case of the Plummer Model

The Plummer lens equation (7) can be rewritten as

$$\zeta = z - \frac{\kappa_0 z}{1 + z\bar{z}}. \quad (26)$$

From the definition of the deflection factor f , it follows that

$$f(z) = \frac{\kappa_0}{1 + \frac{z^2\bar{\zeta}}{\zeta}}. \quad (27)$$

Hence $zf \rightarrow 0$ as $|z| \rightarrow \infty$ and f involves no roots of z and hence no branch cut. The imaging equation is of third degree in z and, since the maximum number of images is three, there are no spurious roots. Thus, the Plummer model has a magnification invariant

$$\sum_{i=1}^3 \mu_i p_i = 1. \quad (28)$$

In other words, the sum of the signed magnifications $\mu_i p_i$ of the images is an invariant of the model. This result appears not to have been realized before.

3 THE PLUMMER MODEL WITH BLACK HOLE

3.1 Lens Equation

The standard Plummer lens is now modified by introducing a point mass m as a model for a black hole at the centre. Using dimensionless coordinates in L as before, its relative surface density is

$$\kappa_{\text{BH}}(\mathbf{w}) = \frac{m}{D_{\text{LO}}^2} \delta^{(2)}(\mathbf{w}), \quad (29)$$

whence the total deflection potential is

$$\Psi(\mathbf{x}) = \Psi_{\text{P}}(\mathbf{x}) + \frac{1}{\pi} \int_L \kappa_{\text{BH}}(\mathbf{w}) \ln |\mathbf{w} - \mathbf{x}| d^2 w \quad (30)$$

$$= \Psi_{\text{P}}(\mathbf{x}) + a \ln x, \quad (31)$$

where $a = m/\pi D_{\text{LO}}^2 \Sigma_{\text{crit}}$. The lens equation follows immediately,

$$\mathbf{y} = \mathbf{x} - \frac{\kappa_0 \mathbf{x}}{1 + \left(\frac{x}{x_0}\right)^2} - \frac{a \mathbf{x}}{x^2} \quad (32)$$

using (6).

3.2 Image and Caustic Properties

This lens equation shows that the point mass introduces an additional image at $\mathbf{x} \rightarrow -a\mathbf{y}/y^2$ as $y \rightarrow \infty$: the minimum number of images is two. Moreover, eq (32) is of fourth degree in x , so a maximum of four images is expected. Some further insight can be gained analytically. With the substitution

$$\frac{x_1}{x_0} = \xi \cos \theta, \quad \frac{x_2}{x_0} = \xi \sin \theta, \quad a_0 = \frac{a}{x_0^2} = \frac{m}{\pi r_0^2 \Sigma_{\text{crit}}} \quad (33)$$

where $\xi \geq 0$, the Jacobian can be constructed from the partial derivatives,

$$\begin{aligned} \frac{\partial y_1}{\partial x_1} &= 1 - \frac{\kappa_0}{1 + \xi^2} + \frac{2\kappa_0 \xi^2 \cos^2 \theta}{(1 + \xi^2)^2} + \frac{a_0(2 \cos^2 \theta - 1)}{\xi^2} \\ \frac{\partial y_1}{\partial x_2} &= \frac{2\kappa_0 \xi^2 \cos \theta \sin \theta}{(1 + \xi^2)^2} + \frac{2a_0 \cos \theta \sin \theta}{\xi^2} = \frac{\partial y_2}{\partial x_1} \\ \frac{\partial y_2}{\partial x_2} &= 1 - \frac{\kappa_0}{1 + \xi^2} + \frac{2\kappa_0 \xi^2 \sin^2 \theta}{(1 + \xi^2)^2} + \frac{a_0(2 \sin^2 \theta - 1)}{\xi^2}. \end{aligned}$$

The radii of the two critical circles are given by $\det J = 0$, which yields:

$$1 - \frac{\kappa_0}{1 + \xi_{\text{crit},1}^2} - \frac{a_0}{\xi_{\text{crit},1}^2} = 0 \quad (34)$$

so that

$$\xi_{\text{crit},1} = \sqrt{\frac{\kappa_0 + a_0 - 1}{2} \pm \sqrt{\left(\frac{1 - (\kappa_0 + a_0)}{2}\right)^2 + a_0}} \quad (35)$$

and

$$1 - \frac{\kappa_0}{1 + \xi_{\text{crit},2}^2} + \frac{2\kappa_0 \xi_{\text{crit},2}^2}{(1 + \xi_{\text{crit},2}^2)^2} + \frac{a_0}{\xi_{\text{crit},2}^2} = 0. \quad (36)$$

The critical circle (35) has precisely one solution for all positive κ_0, a_0 . Applying the lens equation shows that it maps to a caustic point at the origin of S . If $\kappa_0 \leq 1$, there is hence one critical circle in L at $\xi_{\text{crit},1}$ and one caustic point in S : the number of images is always two for $\mathbf{y} \neq \mathbf{0}$. If $\kappa_0 > 1$, $\xi_{\text{crit},2}$ introduces two further critical circles in L and two caustics in S , in contrast to one for the Plummer model. Although (36) is a third degree polynomial in $\xi_{\text{crit},2}^2$ and could in principle be solved analytically, it is, however, more instructive to display the critical circles and caustics numerically. Figure 1 illustrates this case with three critical circles and two

caustic circles, giving rise to an annular domain with four images inside and two outside of it.

3.3 Maximum Black Hole Mass

If the point mass a_0 increases while the Plummer mass κ_0 is kept fixed, the former will eventually dominate the latter, for some $a_0 > a_{0,\text{max}}$. In consequence, two images will occur for all $\mathbf{y} \neq \mathbf{0}$, as is plain from the lens equation for negligible κ_0 . The annulus in S resulting in four images will hence disappear, as shown in Figure 2.

Let us take without loss of generality $\mathbf{y} = (y_1, 0) \Rightarrow x_2 = 0$, then (32) requires for the presence of four images $\kappa_0 > 1$ and four intersections of

$$\xi_1 - \frac{y_1}{x_0} = \frac{\kappa_0 \xi_1}{1 + \xi_1^2} + \frac{a_0}{\xi_1}. \quad (37)$$

where $\xi_1 = x_1/x_0$. At the threshold $\xi_1 = \xi_0$, $a_0 = a_{0,\text{max}}$, the graphs of left-hand side and right-hand side match in first and second derivatives,

$$1 = \frac{\kappa_0(1 - \xi_0^2)}{(1 + \xi_0^2)^2} - \frac{a_{0,\text{max}}}{\xi_0^2} \quad (38)$$

$$0 = \frac{2\kappa_0 \xi_0(\xi_0^2 - 3)}{(1 + \xi_0^2)^3} + \frac{2a_{0,\text{max}}}{\xi_0^3}. \quad (39)$$

Eliminating $a_{0,\text{max}}$, they yield a third degree polynomial in ξ_0^2 which becomes, after the standard substitution $q = \xi_0^2 + 1$,

$$q^3 + 3\kappa_0 q - 4\kappa_0 = 0. \quad (40)$$

Since its cubic determinant is positive, there is one real solution which can be obtained from Cardano's formula,

$$q = (2\kappa_0 + \kappa_0 \sqrt{\kappa_0 + 4})^{1/3} - (\kappa_0 \sqrt{\kappa_0 + 4} - 2\kappa_0)^{1/3} \quad (41)$$

to give, using (39) and (40),

$$a_{0,\text{max}} = \frac{(q - 1)^2(4 - q)}{4 - 3q}. \quad (42)$$

In physical units, the maximum mass of the point mass for four images relative to the Plummer model is

$$\frac{m_{\text{max}}}{M} = \frac{a_{0,\text{max}}}{\kappa_0}. \quad (43)$$

Now consider this as a model of a galaxy with a supermassive black hole. Since many parameters are free, let us take, as a typical example, the total galaxy mass to be $M = 10^{12} M_\odot$ and scale length $r_0 = 10$ kpc. Let the lens and source be at redshifts $z = 0.5$ and $z = 3$, respectively, in an Einstein-de Sitter universe with $H = 70 \text{ km s}^{-1} \text{ Mpc}^{-1}$. This is a sufficient approximation to the Concordance Cosmology for the purpose of estimating parameters here, especially because the source distance at higher redshift almost cancels out. A well-known expression for angular diameter distances (e.g., Peacock 2003, p. 103), then yields $D_{\text{SO}}, D_{\text{SL}}, D_{\text{LO}}$. Hence from the definitions (5), we have:

$$\kappa_0 = \frac{4GM}{c^2 r_0} \frac{D_{\text{SL}} D_{\text{LO}}}{D_{\text{SO}} r_0} = 1.28 > 1 \quad (44)$$

so that four images can occur, provided the mass of the central black hole is less than

$$\frac{m_{\text{max}}}{M} = 4.2 \times 10^{-3} \Rightarrow m_{\text{max}} = 4.2 \times 10^9 M_\odot \quad (45)$$

from (43). In fact, this result is of the same order of magnitude as

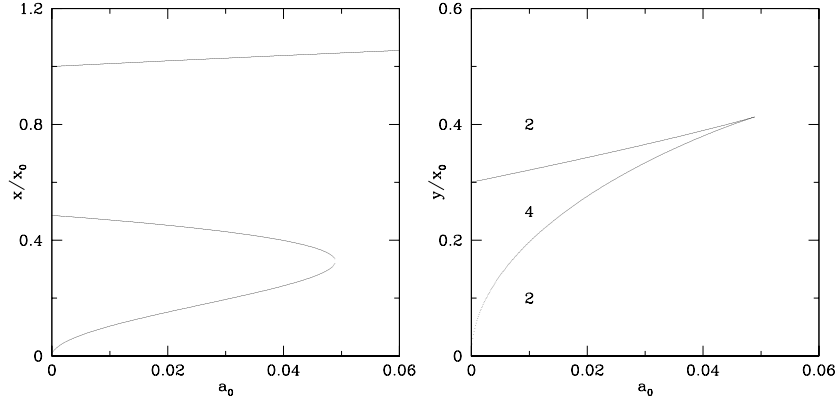


Figure 2. Plummer lens with central point mass, $\kappa_0 = 2$. Left: radii of critical circles in L as function of point mass a_0 , right: radii of caustic circles in S as function of a_0 . Number labels indicate number of images. Note the disappearance of the caustic annulus with four images.

the masses inferred from observations: the presently surmised median mass of supermassive black holes is $(1.4 \pm 0.4) \times 10^{-3}$ of the bulge mass, and galaxy M87 is thought to have a supermassive black hole of mass $(3 \pm 1) \times 10^9 M_\odot$ (Häring & Rix 2004). This indicates that by ascertaining a fourth lensed image, a relevant upper bound on the mass of the supermassive black hole can be obtained. Note also that this method is viable at cosmological distances which are inaccessible to precise mass measurements from stellar kinematics.

However, this approach has two main difficulties: first, it requires knowledge of κ_0 and hence the mass and size of the lens, and secondly, the fourth image may be missed or be misinterpreted. Bowman et al. (2004) have recently considered the lensing properties of a cored and a broken power-law isothermal sphere with central point mass. Because of their diverging masses, these models are only valid centrally and hence a black hole mass bound from lensing, as described here, is not discussed. Based on their numerical simulation of lensing cross-sections, the authors conclude that observations of the fourth image, as characteristic lensing signature of a supermassive black hole, should require the next generation of radio telescopes but nevertheless recommend searching already.

3.4 Magnification Invariant

Using the same conventions as in §2.3, the lens equation (32) can be recast thus

$$\zeta = z - \frac{\kappa_0 z}{1 + z\bar{z}} - \frac{a_0}{\bar{z}} \quad (46)$$

such that

$$f(z) = \frac{\kappa_0}{1 + z^2\bar{\zeta}} + \frac{a_0\zeta}{z^2\bar{\zeta}}, \quad (47)$$

so again $zf \rightarrow 0$ as $|z| \rightarrow \infty$ and f has no branch cut. The maximum number of images is four. Likewise, the imaging equation is of fourth degree in z so there are no spurious roots. Therefore, the magnification invariant holds for the Plummer model with central point mass as well,

$$\sum_{i=1}^4 \mu_i p_i = 1. \quad (48)$$

Although the central black hole has yielded a further image, it is still true that the sum of the signed magnifications is unity.

4 THE PLUMMER LENS WITH BLACK HOLE AND SHEAR

4.1 Lens Equation

Circular symmetry is however normally broken in gravitational lensing. This may be caused by flattening of the lensing galaxy itself or by the presence of an external gravitational field, for instance, in a galaxy cluster. For simplicity, let us consider a constant external mass surface density κ_{ext} and shear γ_{ext} . Let the Cartesian coordinate axes be in the principal directions so that the perturbation of the lens equation is in diagonal form (e.g., Schneider et al. 1999, p. 250)

$$\begin{aligned} \Delta \mathbf{y} &= - \begin{pmatrix} \kappa_{\text{ext}} + \gamma_{\text{ext}} & 0 \\ 0 & \kappa_{\text{ext}} - \gamma_{\text{ext}} \end{pmatrix} \mathbf{x} \\ &= - \begin{pmatrix} \Gamma_1 & 0 \\ 0 & \Gamma_2 \end{pmatrix} \mathbf{x} \end{aligned} \quad (49)$$

where Γ_1, Γ_2 are the components of the total external shear. The lens equation (32) is now modified thus

$$y_1 = x_1 - \frac{\kappa_0 x_1}{1 + \left(\frac{x}{x_0}\right)^2} - \frac{a x_1}{x^2} - \Gamma_1 x_1 \quad (50)$$

$$y_2 = x_2 - \frac{\kappa_0 x_2}{1 + \left(\frac{x}{x_0}\right)^2} - \frac{a x_2}{x^2} - \Gamma_2 x_2. \quad (51)$$

For $\Gamma_1 \neq \Gamma_2$, the imaging equation is a fifth order polynomial in $z\bar{z}$. However, as we will see in the next section, the maximum number of images of a Plummer model with black hole and shear is 6. Hence in general, there are spurious roots to the imaging polynomial and a magnification invariant does not exist.

4.2 Image and Caustic Properties

4.2.1 Astroid Caustic

When $\Gamma_1 = \Gamma_2$, eqns (50) and (51) remain circularly symmetric with three critical circles, two caustic circles and a critical and caustic point, as in §3.

Consider now the case $\Gamma_1 \neq \Gamma_2$, $\Gamma_1 > 0 \wedge \Gamma_2 > 0$, that is, the external mass surface density $\kappa_{\text{ext}} > \gamma_{\text{ext}}$. Since, by construction, the coordinate axes point in the principal directions of the external shear, the critical curves in L intersect the x_1 -axis with a tangent vector parallel to $(0, 1)$ and the x_2 -axis with $(1, 0)$. The corresponding caustic tangent vanishes if, in addition, $\partial y_2 / \partial x_2 = 0$

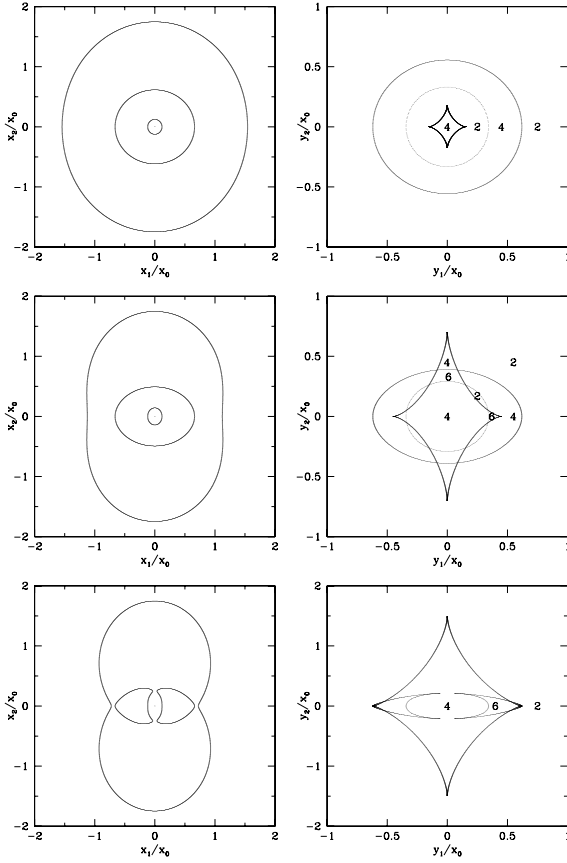


Figure 3. Plummer lens with point mass and external shear, $\kappa_0 = 2$, $a_0 = 0.02$. The difference between the components of external shear increases from top to bottom. Upper left: critical curves, upper right: caustics, for $\Gamma_1 = 0.5$, $\Gamma_2 = 0.4$. Middle left: critical curves, middle right: caustics, for $\Gamma_1 = 0.5$, $\Gamma_2 = 0.1$. Lower left: critical curves, lower right: caustics, for $\Gamma_1 = 0.5$, $\Gamma_2 = -0.35$. Number labels indicate number of images.

or $\partial y_1 / \partial x_1 = 0$, respectively. Then, these are *cusp points* on the y_1, y_2 -axes in S (e.g. (Schneider et al. 1999), p. 252). They may be categorised thus:

- Cusp points on y_1 -axis: $x_2 = 0 \wedge \frac{\partial y_2}{\partial x_2} = 0$

$$\Rightarrow 0 = 1 - \frac{\kappa_0}{1 - \Gamma_2} \frac{1}{1 + (\frac{x_1}{x_0})^2} - \frac{a}{1 - \Gamma_2} \frac{1}{x_1^2} \text{ from (51)}$$

$$\Rightarrow y_1 = x_1(\Gamma_2 - \Gamma_1) \text{ from (50)}$$

There is precisely one solution for x_1^2 , hence precisely two for x_1 and two for y_1 since $\Gamma_1 \neq \Gamma_2$.

- Cusp points on y_2 -axis: $x_1 = 0 \wedge \frac{\partial y_1}{\partial x_1} = 0$

$$\Rightarrow 0 = 1 - \frac{\kappa_0}{1 - \Gamma_1} \frac{1}{1 + (\frac{x_2}{x_0})^2} - \frac{a}{1 - \Gamma_1} \frac{1}{x_2^2} \text{ from (50)}$$

$$\Rightarrow y_2 = x_2(\Gamma_1 - \Gamma_2) \text{ from (51)}$$

Again, there is precisely one solution for x_2^2 , hence precisely two for x_2 and two for y_2 since $\Gamma_1 \neq \Gamma_2$.

Therefore, $\Gamma_1 \neq \Gamma_2$ lifts the degeneracy of the caustic point at $\mathbf{y} = \mathbf{0}$ which was found the previous circularly symmetric cases. There is now one pair of cusp points on each of the y_1, y_2 -axes giving rise to an *astroid* caustic. By crossing the astroid inwards, the number of images increases from two to four. If the point source

is at $\mathbf{y} = \mathbf{0}$, an additional fifth image at the centre of L is produced, since by (50) and (51) $\mathbf{x} = \mathbf{0}$ is a solution. Note that, in this case, circular symmetry is broken and an Einstein ring image cannot form. The astroid increases in size as Γ_1, Γ_2 become more different, eventually intersecting the already existing caustic curves. Caustic domains are thereby created in which the image multiplicity increases from a maximum of four to six. Such a configuration of critical and caustic curves is illustrated in the upper and middle panel of figure 3.

4.2.2 Metamorphoses

As the difference in the shear components increases yet further, $\Gamma_1 > 0 \wedge \Gamma_2 < 0$ and the external mass surface density $\kappa_{\text{ext}} < \gamma_{\text{ext}}$. Now critical curves and caustics rejoin, as can be seen in the lower panel of figure 3: as the inner two critical curves in L merge on the x_2 -axis, the tangent vector vanishes and $\nabla \det J = 0$. This corresponds to the rejoining of the inner two caustics on the y_2 -axis to give two cusps, and is an example of a beak-to-beak metamorphosis.

Our model can also serve to illustrate the metamorphosis of an umbilic. Referring to the deflection potential Ψ in equation (31) and the lens equation with external shear (50), (51), the conventional form (e.g., Schneider et al. 1999, p. 162) of the Jacobian J of the lens mapping is,

$$J = \begin{pmatrix} 1 - \kappa - \gamma_1 & -\gamma_2 \\ -\gamma_2 & 1 - \kappa + \gamma_1 \end{pmatrix} \quad (52)$$

where

$$\gamma_1 = \frac{1}{2} \left(\frac{\partial^2 \Psi}{\partial x_1^2} - \frac{\partial^2 \Psi}{\partial x_2^2} \right) + \gamma_{\text{ext}}$$

$$\gamma_2 = \frac{\partial^2 \Psi}{\partial x_1 \partial x_2}$$

$$\kappa = \frac{1}{2} \left(\frac{\partial^2 \Psi}{\partial x_1^2} + \frac{\partial^2 \Psi}{\partial x_2^2} \right) + \kappa_{\text{ext}}.$$

The umbilic point occurs where both eigenvalues λ_1, λ_2 of J vanish,

$$\lambda_1 = 1 - \kappa + \sqrt{\gamma_1 + \gamma_{\text{ext}}} = 0$$

$$\lambda_2 = 1 - \kappa - \sqrt{\gamma_1 + \gamma_{\text{ext}}} = 0.$$

These two conditions can now be applied to derive the location of umbilic metamorphoses. Since, by construction, the coordinate system in the lens plane is aligned with the principal directions of external shear, we can set $\Gamma_1 > \Gamma_2$ and $x_2 = 0$. Then keeping κ_0, a_0, Γ_1 fixed defines a one-parameter family of lens models in Γ_2 . Letting $\xi_1 = x_1/x_0$, we hence obtain the value of Γ_2 for the metamorphosis from

$$\begin{aligned} \frac{\kappa_0(1 - \xi_1^2)}{(1 + \xi_1^2)^2} - \frac{a_0}{\xi_1^2} &= 1 - \Gamma_1 \\ \frac{\kappa_0}{1 + \xi_1^2} + \frac{a_0}{\xi_1^2} &= 1 - \Gamma_2. \end{aligned}$$

Figure 4 illustrates the caustics for a particular Plummer model with central point mass and external shear undergoing metamorphosis at an umbilic point.

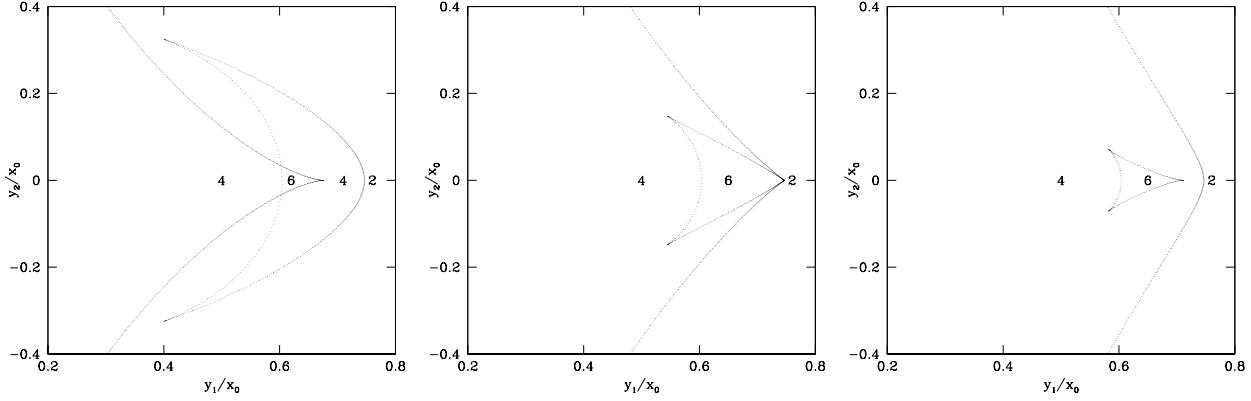


Figure 4. Caustics for the Plummer lens with central point mass and external shear, $\kappa_0 = 2$, $a_0 = 0.06$, $\Gamma_1 = 0.6$. The difference between the components of external shear increases left to right as Γ_2 decreases. Left: $\Gamma_2 = -0.1$, middle: $\Gamma_2 = -0.52$ where the umbilic metamorphosis occurs, right: $\Gamma_2 = -0.9$. Number labels indicate number of images.

5 CONCLUSION

This paper provides an analytic study of the lensing properties of the Plummer model, together with modifications incorporating the effects of a central point mass and external shear. This is a simple model for lensing by a flattened galaxy with a central black hole. The maximum number of images given by the circular Plummer lens is 3. This number rises to 4 if a central point mass is introduced and to 6 if external shear is added as well.

There are three new results of our work. First, a magnification invariant is found to exist for both the Plummer lens alone, and for the Plummer lens with black hole. Even though the introduction of a black hole changes the maximum number of images from 3 to 4, it is nonetheless true that the sum of the signed magnifications remains unity.

The second result is a treatment of the caustic structure for the Plummer lens with black hole and shear. Without shear, there are two caustic circles and a caustic point. This gives three disjoint regions in the source plane where double, quadruple and double imaging respectively occur. The introduction of shear causes the caustic point to unfold as an astroid caustic. The presence of four cusps on an astroid caustic is established, demonstrating the change of image multiplicities as the caustics intersect and metamorphoses occur. For modest shear, the astroid is contained within the two outer caustics. However, as the components of shear Γ_1 and Γ_2 become more different, the size of the astroid increases and additional caustic domains are created in which the image multiplicity is 6.

Based on this discussion of caustic curves, we describe a possible method to obtain an upper limit on the mass of a black hole from gravitational lensing. As this approach relies on counting images alone, it could be used at cosmological distance and therefore as an independent check on mass estimates obtained from other methods, such as stellar kinematics and reverberation mapping. This emphasises the value of lensing surveys for constraining the mass distribution in the inner parts of galaxies.

ACKNOWLEDGMENTS

MCW gratefully acknowledges PPARC funding.

REFERENCES

- An J.H., Evans N.W., 2006, MNRAS, submitted
- Binney J., Tremaine S., 1987, Galactic Dynamics, Princeton University Press, Princeton
- Bowman J. D., Hewitt J. N., Kiger J. R., 2004, ApJ, 617, 81
- Einstein A., 1911, Ann. Phys., 35, 898
- Evans, N. W., & Hunter, C. 2002, ApJ, 575, 68
- Evans N. W., Wilkinson M. I., 1998, MNRAS, 296, 800
- Häring N., Rix H., 2004, ApJ, 604, L89
- Hunter C., Evans N. W., 2001, ApJ, 554, 1227
- Keeton C. 2003, ApJ, 582, 17
- Mao S., Witt H. J., Koopmans L. V. E., 2001, MNRAS 323, 301
- Peacock J., 2003, Cosmological Physics, Cambridge University Press, Cambridge
- Petters A. O., Levine H., Wambsganns J., 2001, Singularity Theory and Gravitational Lenses, Birkhäuser, Boston
- Rhie S. H., 1997, ApJ, 484, 63
- Schneider P., Ehlers J., Falco E., 1999, Gravitational Lenses, Springer, Berlin
- Walsh D., Carswell R. F., Weymann R. J., 1979, Nat, 279, 381
- Witt H. J., Mao S., 1995, ApJ, 447, L105
- Witt H. J., Mao S., 2000, MNRAS, 311, 689
- Zwicky F., 1937, Phys. Rev., 51, 290